Studies on structural and optical properties of ZnO and Mn-doped ZnO nanopowders

Arun S Menon, Nandakumar Kalarikkal and Sabu Thomas

Centre for Nanoscience and Nanotechnology, Mahatma Gandhi University, Kottayam, Kerala 686 560*, India*
arunsmenon15@gmail.com

Abstract

Well-crystalline ZnO nanoparticles (NPs) were synthesized in large-quantity via sol-gel process using the mixtures of zinc acetate and citric acid. The detailed structural properties were examined using x-ray diffraction pattern (XRD) and scanning electron microscope (SEM) which revealed that the synthesized nanoparticles are well-crystalline and possessing wurtzite hexagonal phase. Crystalline size, lattice parameters, unit cell volume and atomic packing fraction were determined from the obtained XRD data. The presence of functional groups in the samples was observed from FTIR spectra. The optical properties were studied by using UV visible spectroscopy. The nanoparticles are almost spherical shape with the average diameters of 15±10 nm.We also tried to study the effect on the structural and optical properties ofMn doped ZnO nanoparticles. The absorption edge shifts towards lower energy upto0.1 at% doping concentration and shifts to higher energy when the Mn doping concentration increasesupto 0.2at% due to Burstein-Moss effect.

Keywords: ZnO, Doped ZnO, Sol gel, Burstein-Moss effect.

1. Introduction

Nanomaterials are fascinating due to their smaller particle size and large surface area (Yadav *et al.,* 2007). Among these nanomaterials, ZnO nanostructures are promising candidates for wide range of applications from optoelectronics to variety of sensors (Erol *et al.,* 2010). ZnO, a n-type II-VI compound semiconductor, direct and wide band gap of 3.44eV at low temperature and 3.37eV at room temperature, high efficient UV emission resulting from a large exciton binding energy, 60 MeV, at room temperature, high specific area, fine particle size, quantum confinement properties, non-toxic, inexpensive, mechanically stable, high resistant to deoxidation (Li Liu *et al.,* 2011; Hassan Karami, 2010; Anderson Janotti & Chris G Van de Walle, 2009). Surface area and surface defects play an important role in many applications such as sensing and photocatalytic activities (Ruhullah & Joy deep Dutta, 2008). Doping of metal oxide and/or transition metals [like Mn] increases the surface defects. In addition, it affects the optical and electronic properties and can presumably shift the optical absorption towards the visible region (Rekha *et al.,* 2010). In the case of wide band gap semiconductors, electrical conductivity is mainly due to the intrinsic defects such as interstitial zinc atoms and oxygen vacancies. Hence doping drastically changes their electrical and optical properties (Ellmer *et al.,*1994).

Various techniques have been used to synthesize ZnO and doped ZnO nanoparticles and can be categorized into either liquid-solid or gas-solid nature of transformation. Co-precipitation method, sol-gel processing, microemulsion technique, solvothermal methods etc. are some of the liquid-solid type synthesis. Chemical vapor deposition and pulsed laser deposition are examples of gas-solid type of transformation [9-10]. Among these methods of synthesis, solution based approach is simplest, but solvent and the precursor as well as reaction conditions such as pH, temperature and time need to be controlled properly to achieve the morphology of the nanostructure [11].Synthesis and processing of nanomaterialsis an essential aspect. It is necessary to note that smaller crystal size of nanocrystals does not necessarily mean the enchancement in all applications especially like gas sensing [12].

In this study, we report synthesis of zinc oxide and manganese doped zinc oxide nanoparticles by using sol-gel technique. The crystalline structure and morphology of the samples was investigated with x-ray diffractometer (XRD) and scanning electron microscopy (SEM) respectively. The presence of functional groups was observed from FTIR spectra. The optical studies were done by UV-visible spectroscopy and the studies reveal that there occurs a band gap narrowing and band gap widening with respect to Mott critical density. The band gap widening is due to Burstein-Moss effect.

2. Experiment

ZnO nanoparticles and Mn doped ZnOnanoparticles were synthesized following, with minor modification, the method described by Murphy et. Al. Stoichiometric amounts (x=0, 0.05, 0.1, 0.15,0.2) of zinc acetate and manganese acetate along with citric acid were dissolved in 60 mL of water and add ammonium hydroxide up to pH value 7. The mol ratio of zinc acetate and citric acid is 1:1. This mixture is stirred for 6 h to make a sol which was then placed in an oven for 20 h at 95^{o} C to form gel. The gel is placed in a high temperature furnace at 450^{o} C for 4 h where it was cracked to produce the nanopowders.

3. Result and Discussion

3.1 Structural Properties

3.1.1 XRD analysis

Figure 1a-e. shows the XRD pattern of pureZnOand Mn doped ZnO nanoparticles with different concentrations. The crystal structure,grain size, lattice parameters 'a' and 'c', unit cell volume and atomic packing factor were analyzed. Miller indices (1 0 0), (0 0 2) and (1 0 1) for 31.9°, 34.6° and 36.4° respectively were the strongest XRD peaks obtained for ZnO which is confirmed with the JCPDS (card number 36-1451) data. No peaks corresponding to impurities were detected. The average crystallite size is determined by using Debye- Scherrer equation:

$$D = k\lambda / \beta \cos\theta \quad (1)$$

Wherek=0.89, a constant, λis wavelength of X-rays, β is full width at half maximum (FWHM) and θ is the diffraction angle.

Fig.1. *XRD diffraction patterns of $Zn_{1-x}Mn_xO$ (x=0.00, 0.05, 0.1, 0.15, 0.2) respectively*

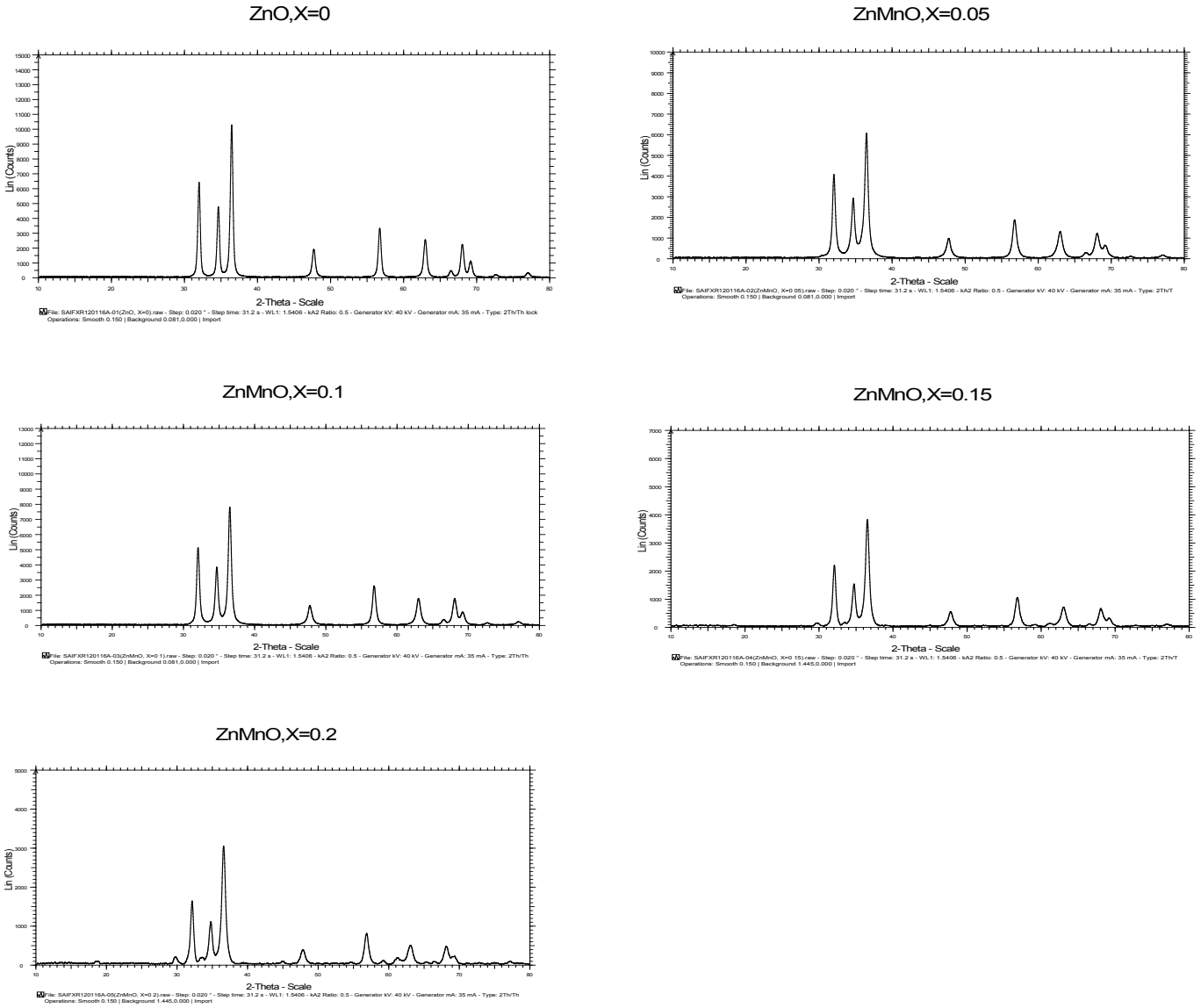

The value of lattice parameters a and c for pure ZnO and Mn doped ZnO were estimated from the equation

$$\frac{1}{d^2_{(hkl)}} = \frac{4}{3}\left[\frac{h^2 + hk + k^2}{a^2}\right] + \frac{l^2}{c^2} \quad (2)$$

where h, k and l are the Miller indices and $d_{h\,k\,l}$ is the interplanar spacing for the plane (h k l). The interplanar spacing can be calculated from Bragg's equation:

$$2d \sin\theta = n\lambda \quad (3)$$

The volume of the unit cell for hexagonal system is obtained from the equation

$$V = 0.866a^2c \quad (4)$$

The number of unit cells in the particle is calculated from the equation:

$$N = \frac{4}{3\pi\frac{D}{2V}} \quad (5)$$

Table 1. *Data on crystalline size, lattice parameters, atomic packing fraction, volume of a unit cell and strain of the samples*

Sample name	Crystalline size (nm)	a (A°)	c (A°)	APF	Cell volume $(A^o)^3$	Strain
Pure ZnO	20.599	3.227	5.174	0.7539	46.66	0.5904
0.05	15.583	3.231	5.178	0.7538	46.81	0.0343
0.1	16.429	3.233	5.181	0.7534	46.89	0.0088
0.15	14.879	3.223	5.166	0.7539	46.47	0.0297
0.2	14.729	3.217	5.159	0.7537	46.25	0.0354

Table 1.shows the obtained values of the samples.The obtained XRD pattern is in good agreement with standard data available in JCPDS (card number 36-1451). The diffraction peaks revealed the presence of hexagonal (wurtzite) structure in all the samples. Average crystalline size is found to be ~16 nm.Value of lattice parameters increased with increase in dopant concentration upto 0.1 at% Mn concentration, then the value of lattice parameters is found to be decreased. The decrease in lattice parameter is caused due to zinc vacancies (Khalid *et al.,* 2009).Manganese can exist in Mn^{2+}, Mn^{3+}, and Mn^{4+}. The ionic radius of Mn^{2+}, Mn^{3+} and Mn^{4+} are 0.66A°, 0.58A° and 0.53A° respectively. The doping concentration increases upto 0.1 the lattice parameters 'a' and 'c' increases due to smaller ionic radius of Zn ($0.6A^0$) than that of Mn^{2+}. Above that concentration level Zn^{2+} is substituted by Mn^{3+} and Mn^{4+} (Bhatti *et al.,* 2005). We also note that this report have been supported by Dole et al. (2011). Atomic packing fraction (APF) were determined and showed in Fig.2, the values of APF decreasing as Mn content increases upto 0.1. and are in good agreement with literature (Sharma *et al.,*2007). The cell volume (average ~46.62A°) confirms the ZnO and Mn doped ZnO has hexagonal structure. It is observed that the strain value decreases upto the doping concentration 0.1 and then the value increases. It is clear that the crystallinity and number of unit cells present in the particle increases in heavy doping (above x=0.1), so the strain value increases.

Fig.2. *Atomic packing fraction vs concentration*

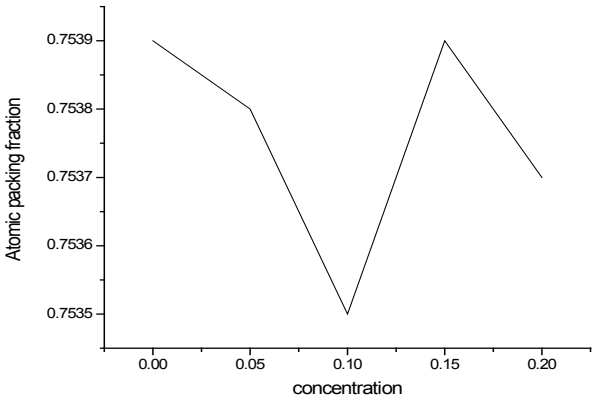

Fig.3 shows the SEM micrographs of pure ZnO and Mn doped ZnO, doped at different doping concentration (x=0.05, 0.1, 0.15 and 0.2). It is clear from the SEM images that the spherical shaped nanoparticles are agglomerated with varying sizes ranging from

14-21 nm. It is seen that the particle size decreases when the doping concentration increases. The SEM images clearly show that the as prepared ZnO and doped ZnOhave porosity to some extent. Fig.4 shows the EDAX spectrum of all the prepared samples and it confirmed the presence of zinc oxide and manganese doped zinc oxide.

Fig.3. *SEM images of (a) Pure ZnO (b) 0.05 Mn doped ZnO (c) 0.1 Mn doped ZnO (d) 0.15 Mn doped ZnO (e) 0.2 Mn doped ZnO*

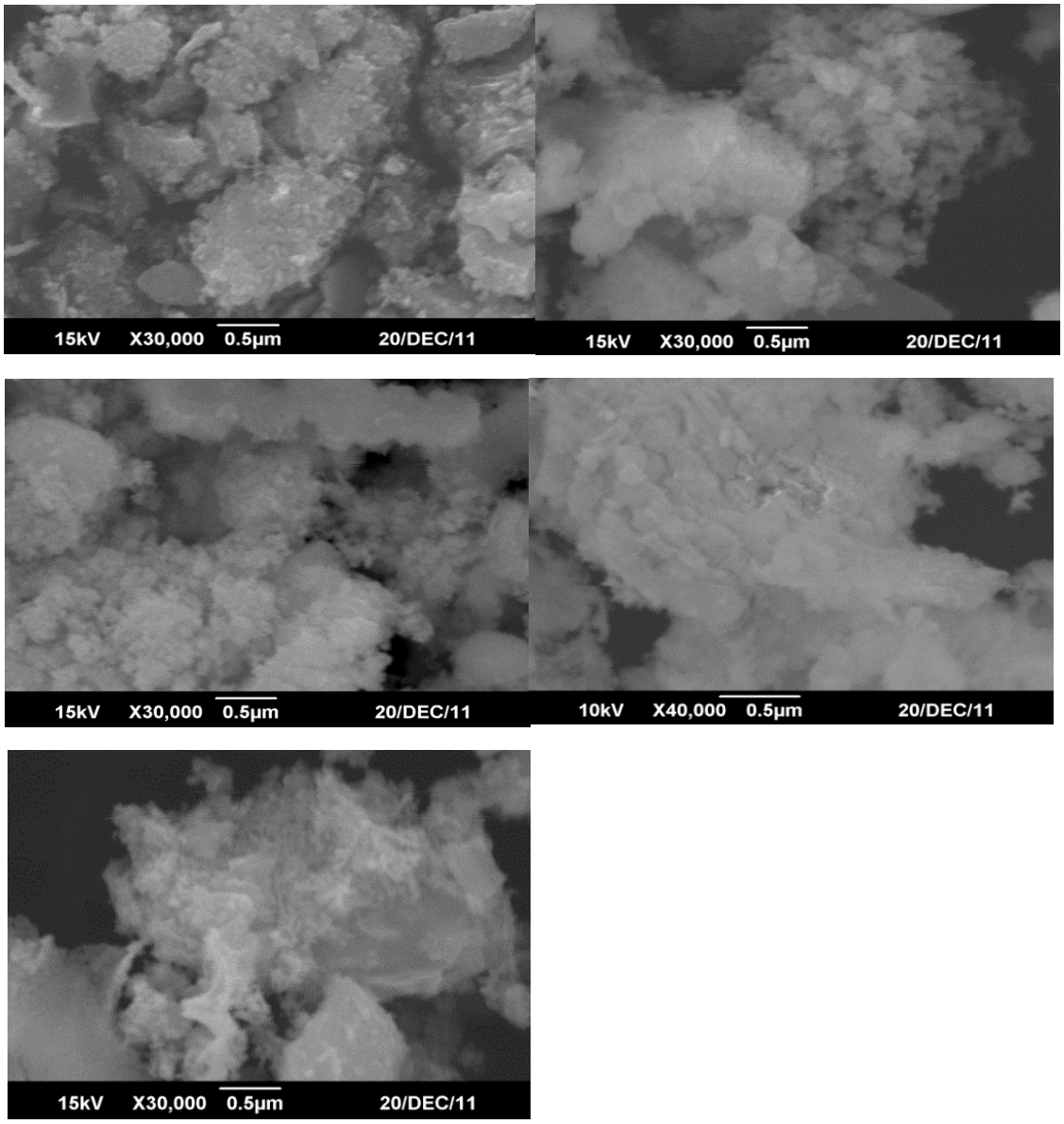

Fig.4. *EDAX spectrum of (a) Pure ZnO (b) 0.05 Mn doped ZnO (c) 0.1 Mn doped ZnO (d) 0.15 Mn doped ZnO (e) 0.2 Mn doped ZnO*

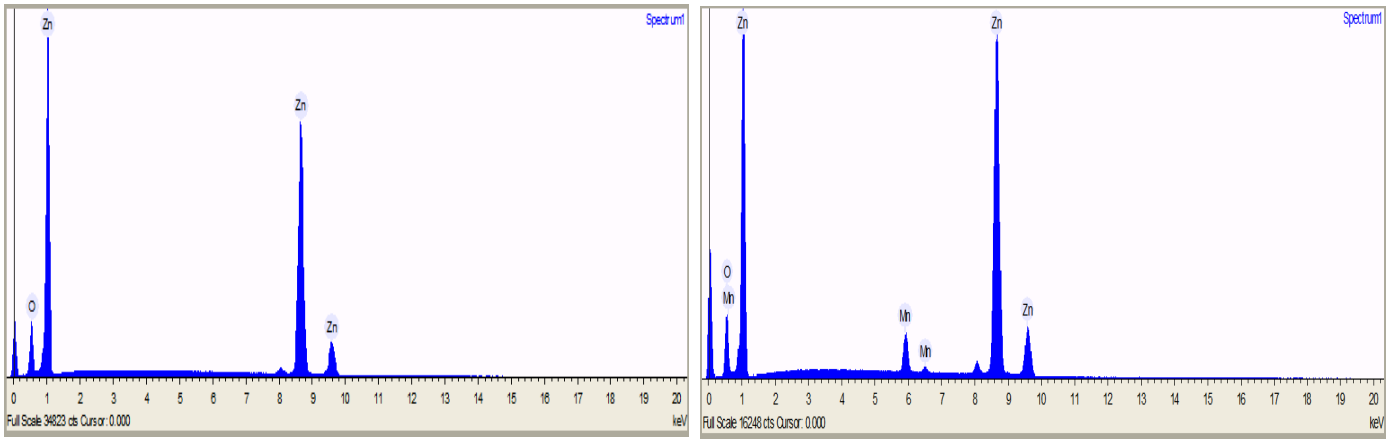

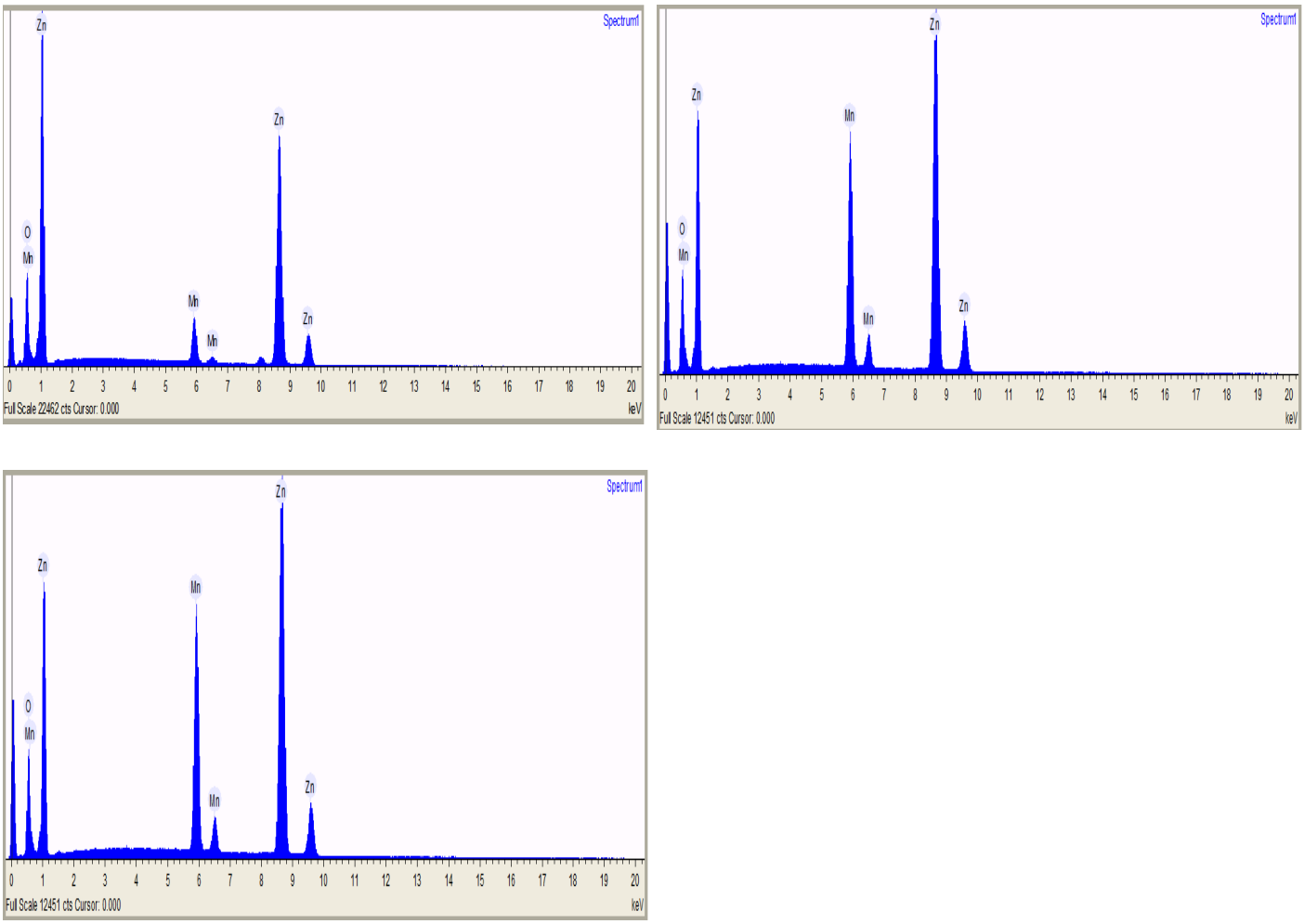

3.1.2 FTIR studies

Fig.5 shows FTIR spectrum of the as prepared pure ZnO and Mn doped ZnO with different doping concentration (x= 0.05, 0.1, 0.15 and 0.2). The peak at ~440 cm^{-1} is due to Zn-O stretching vibration (Kajbafvala *et al.,* 2009). It is clear from the FTIR spectrum that there are no peaks on 3400 cm^{-1} and 1620cm^{-1}. There is no O-H stretching vibrations and H-O-H bending vibration, so the as prepared samples are pure and well suited for any device fabrication.

Fig.5. *FTIR spectra of* $Zn_{1-x}Mn_xO$ *(x=0.00, 0.05, 0.1, 0.15, 0.2) respectively.*

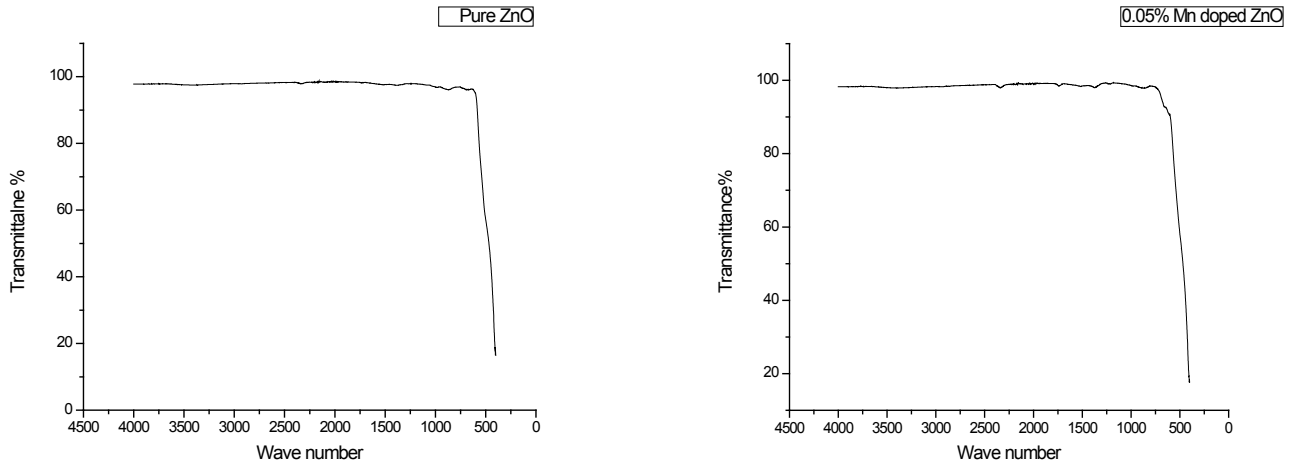

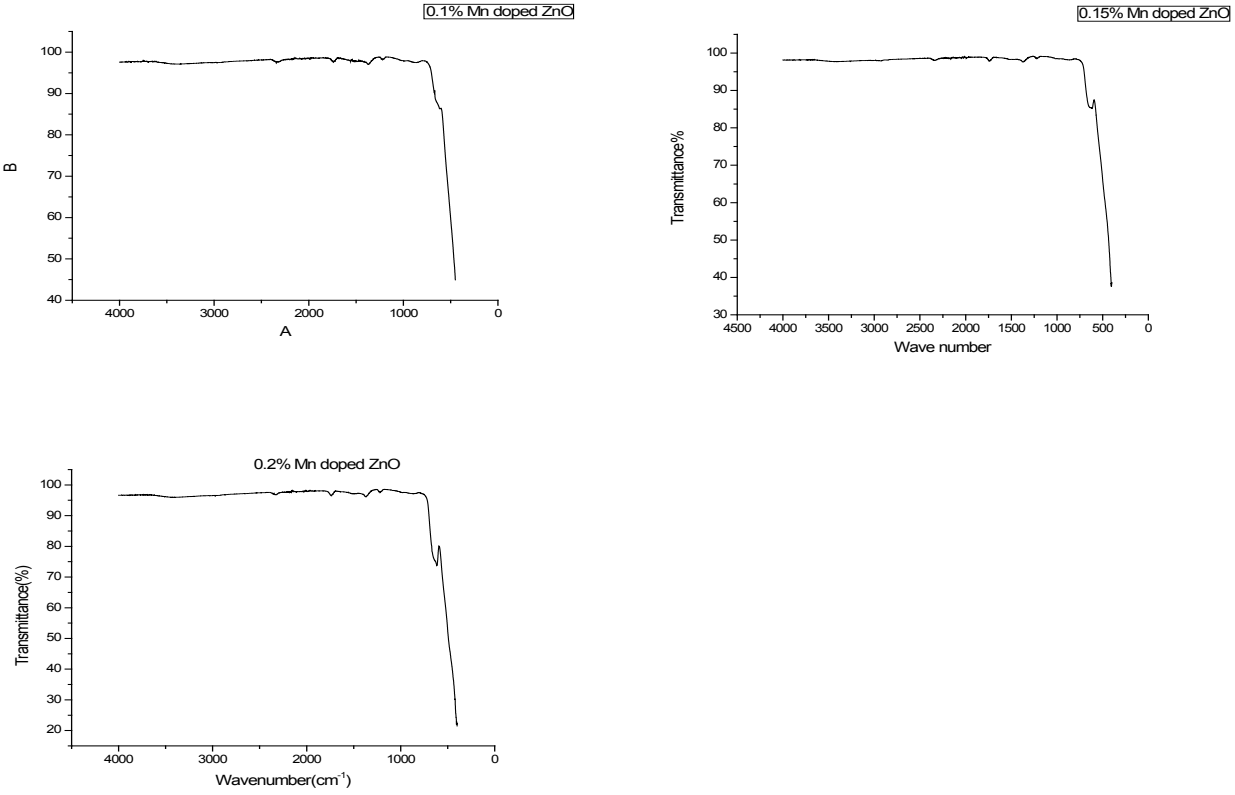

3.2 Optical Properties

3.2.1 UV analysis

Absorption of light by the semiconductor nanoparticles can be tailored by varying the energy band gap and the doping concentration. Fig.6 (a-e) shows absorption spectra of ZnO and Mn doped ZnO (0.05, 0.1, 0.15 and 0.2%) respectively. The optical absorption spectra were recorded in the wavelength region of 300-800nm. From these figures, it is clear that the absorption wavelength varies according to the change in doping concentration [16]. The absorption edge shifts towards higher wavelength when the doping concentration increases. This indicates that the band gap of ZnO material decreases with the doping concentration upto some critical level which is known as Mott critical density. Above Mott critical density the absorption edge shifts towards the lower wavelength region. The lower wavelength shift or increase in the band gap or blue shift can be explained by the Burstein-Moss effect [13,14,15]. The Burstein–Moss effect is the process by which the apparent bandgap of a semiconductor is increased as the absorption edge is pushed to higher energies as a result of all states close to the conduction band being populated. Increase in the dopant concentration leads to the supply of excess carriers which cause the increase band gap or blue shift. In Burstein-Moss effect the Fermi level merges into the conduction band with increase of doping concentration.

Fig.6. *UV absorption spectra of $Zn_{1-x}Mn_xO$ (x=0.00, 0.05, 0.1, 0.15, 0.2) respectively.*

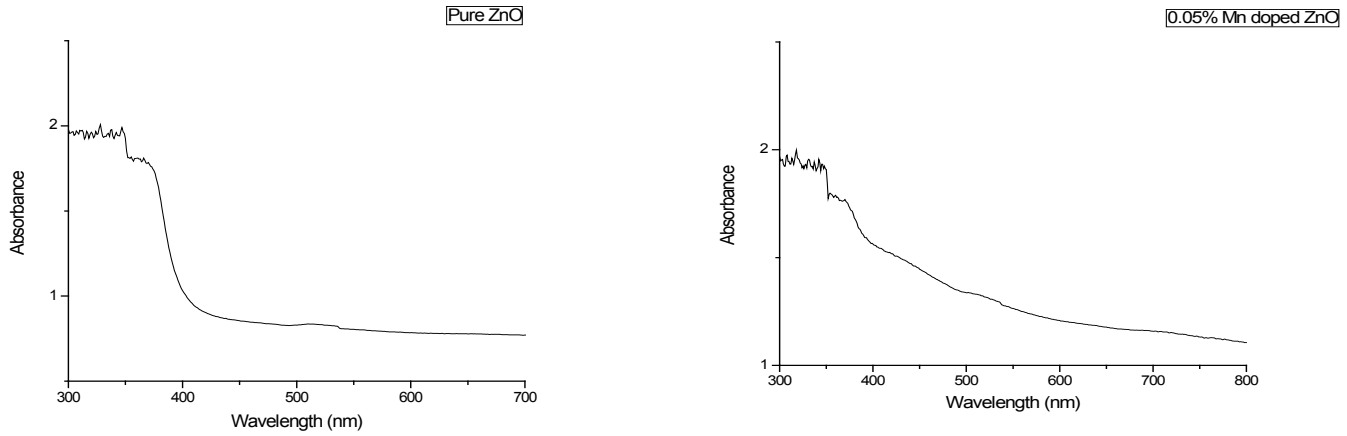

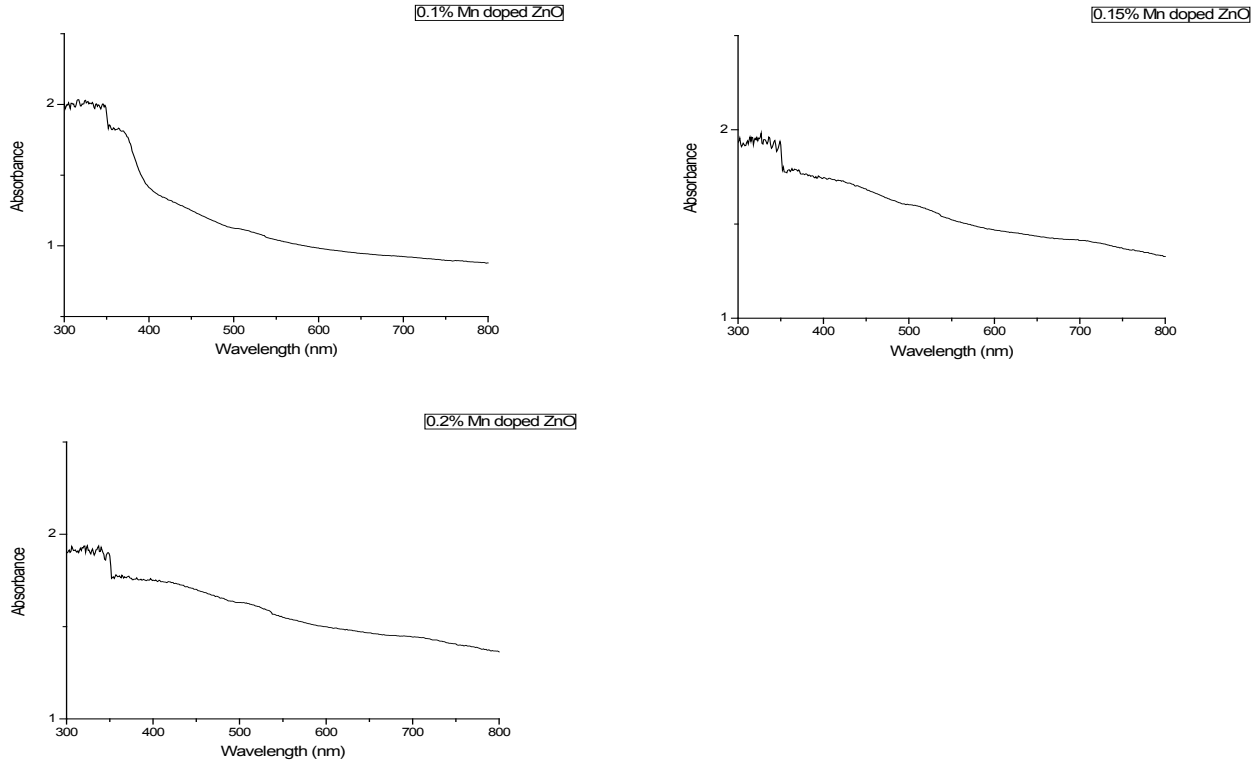

Optical band gap of the samples is determined using the following equation.

$$(\alpha h\nu)^{1/n} \sim (h\nu - E_g) \qquad (6)$$

where α is the absorption coefficient, hν is the photon energy, E_g is the optical band gap and n is the integer whose value depends on the nature of transition. Value of n is 1/2, 2, 3/2 and 3 for direct transition, indirect transition, forbidden direct transition and forbidden indirect transition respectively. The optical band gap was determined from the graph Fig.6. The intercept of this plot on the energy axis gives the energy band gap of the samples. In this case ZnO, 0.05 Mn doped ZnO, 0.1Mn doped ZnO, 0.15 Mn doped ZnO and 0.2 wt% Mn doped ZnOshows the band gap of 3.25,3.2,3.7.3.72 and 3.73eV respectively. The obtained data is well suited with the reported literature (Stroyuk *et al.*,2005).

Fig.7. *Band gap of$Zn_{1-x}Mn_xO$ (x=0.00, 0.05, 0.1, 0.15, 0.2) respectively*

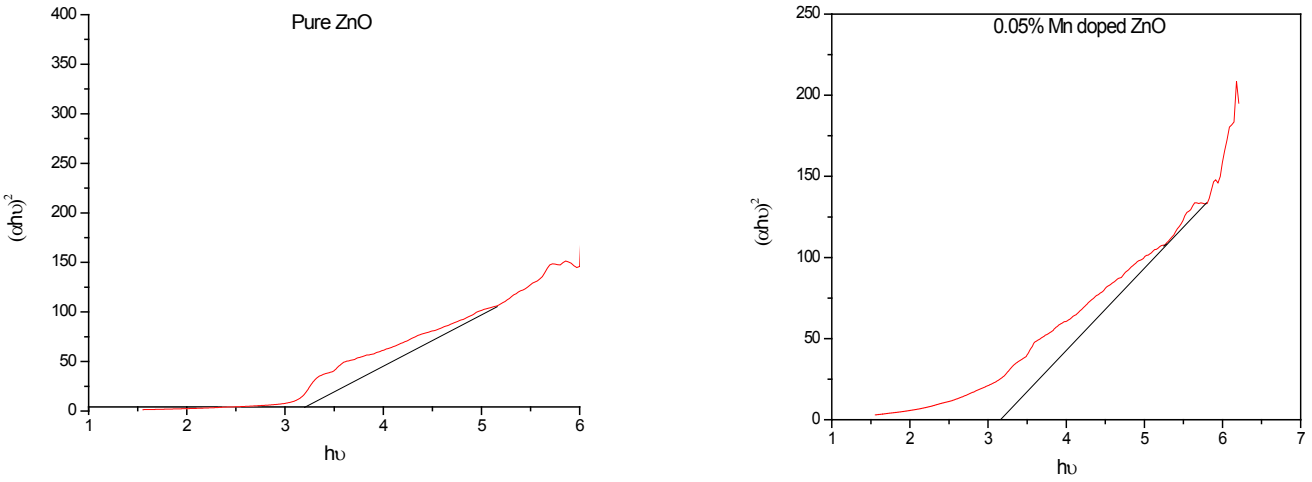

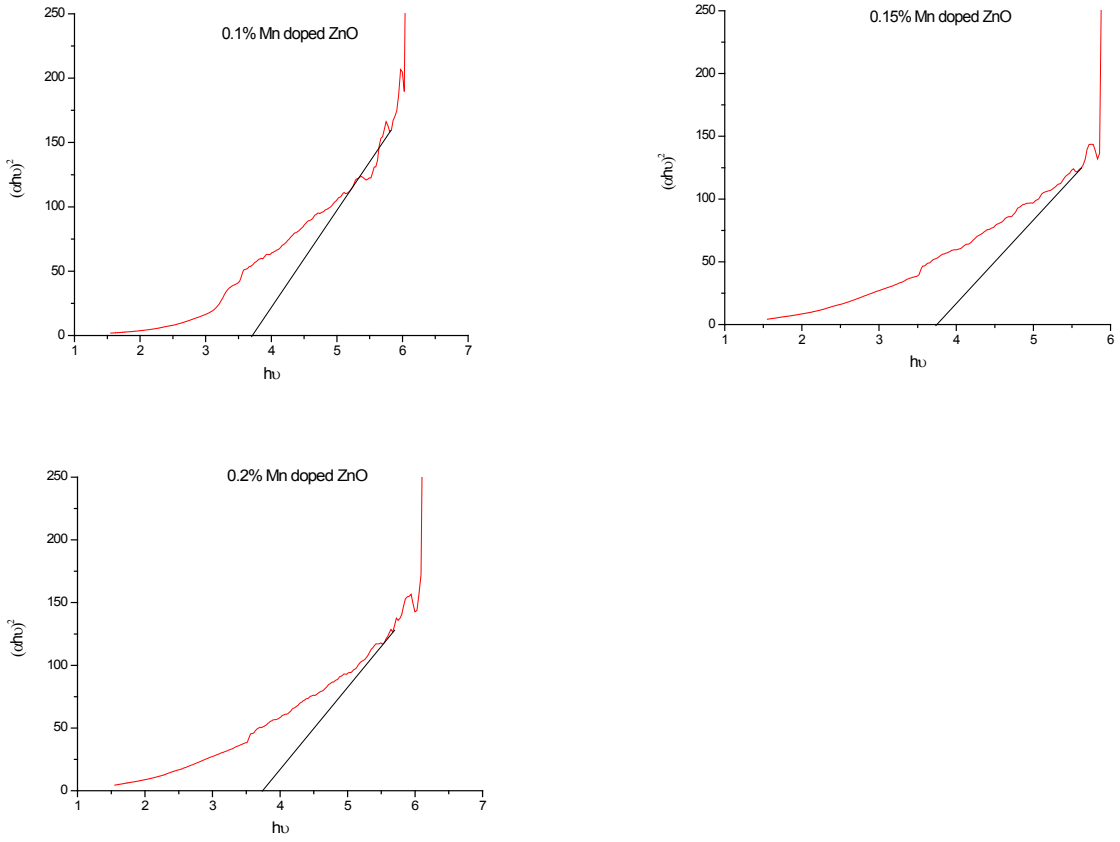

3.2.2 Photoluminescence studies

Fig.8 shows the photoluminescence spectra of pure ZnO and Mn doped ZnO with different dopant concentration. The PL spectra of undoped and Mn doped Zno exhibit blue emission (at 460 nm). The blue emission is because of intrinsic defects such as oxygen and zinc interstitials. The emission in the range of 460-490 nm is due to the presence of Mn ions in ZnO matrix (Viswanatha *et al.,* 2004). The emission was broad and this might be due to phonon-assisted transition (Reynolds *et al.,*1997). This emission was due to the transition from conduction band to acceptor level corresponding to the oxygen antisite (Vimalkumara *et al.,* 2011). It is also observed that the samples exhibits low resistivity after doping, confirms by the blue-green emission intensity decreased when the doping ratio increases.

Fig.8. *Photoluminescence spectra of* $Zn_{1-x}Mn_xO$ *(x=0.00, 0.05, 0.1, 0.15, 0.2) respectively*

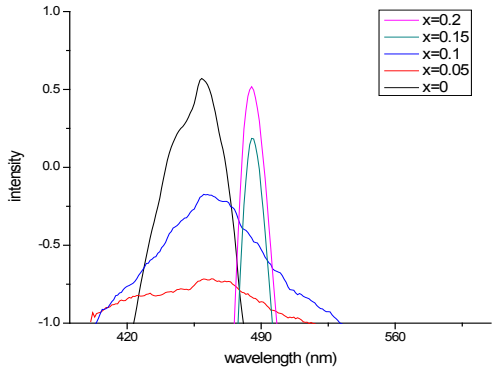

4. Conclusions

Well crystalline zinc oxide and manganese doped ZnO was successfully synthesized by sol-gel method. It is observed that all the samples are in the hexagonal wurtzite structure. The lattice parameters 'a' and 'c' varies when the doping concentration changes. The EDAX spectrum confirms the presence of Mn on ZnO host matrix. The optical absorption studies of ZnO and Mn doped ZnO have been presented. The shift in the absorption edge towards lower wavelength, with increasing the Mn concentration may be attributed

to Burstein-Moss effect. PL spectra shows the blue-green emission of all the samples.

5. References

1. Yadav BC, RichaSrivastava and Alok Kumar (2007) Characterization of ZnO nanomaterial synthesized by different methods. Int. J. Nanotechnol. Applications. 2(2007)
2. Erol A, Okur S, Comba B, Mermer O and Arikan MC (2010) Humidity sensing sensing properties of ZnO nanoparticles synthesized by sol-gel process,. Sensors and Actuators B 145, 174-180.
3. Li Liu, Shouchun Li, Juan Zhuang, Lianyuan Wang, Jinbao Zhang, Haiying Li, Zhen Liu, Yu Han, Xiaoxue Jiang and Peng Zhang (2011) Improved selective acetone sensing properties of Co-doped ZnO nanofibers by electrospinning. Sensors and Actuators B: Chemical. 155 (2), 782-788.
4. Hassan Karami (2010) Invesigation of sol-gel synthesized CdO-ZnOnanocomposite for CO gas sensing. Int. J. Electrochem. Sci.5, 720-730
5. Anderson Janotti and Chris G Van de Walle (2009) Fundamentals of zinc oxide as a Semiconductor. Rep. Prog. Phys. 72,126501
6. Ruhullah and Joy deep Dutta (2008) Photocatalytic degradation of organic dyes with manganese-doped ZnO nanoparticles. J.Hazardous Materials. 156, 194–200
7. Rekha K, Nirmala M, Manjula G Nair and Anukaliani A (2010) Structural, optical, photocatalytic and antibacterial activity of zinc oxide and manganese doped zinc oxide nanoparticles. Physica B. 405, 3180–3185
8. Ellmer K, Cebulla R and Wendt R (1994) Transparent and conducting ZnO: Al films deposited by simultaneous RF- and DC-excitation of a magnetron. Thin Solid Films 317, 413-416
9. Ohring M (1992) The material science of thin films. Academic-Press: San Diego
10. Hubler GK (1992) Pulsed laser deposition. Mater. Res. Bull. 17(2), 25
11. Prantik Banerjee, SampaChakrabarti, SaikatMaitra and Binay K Dutta (2012) Zinc oxide nano-particles -sonochemical synthesis, characterization and application for photo-remediation of heavy metal. Ultrason. Sonochem. 19(1), 85-93
12. Chengxiang Wang, Longwei Yin, Luyuan Zhang, Dong Xiang and RuiGao (2010) Metal Oxide Gas Sensors: Sensitivity and Influencing Factors. Sensors.10, 2088-2106
13. Sumetha Suwan boon, Tunattha Ratana and Walailak Thanakorn Ratana (2007) Title.? J. Sci. Technol. 4 (1), 111
14. Rekha K, Nirmala M, Manjula G and Anukaliani A (2010) Structural, optical, photocatalytic and antibacterial activity of zinc oxide and manganese doped zinc oxide nanoparticles. Physica B. Physics of Condensed Matter. 405 (15) 3180-3185
15. Geeta Sharma, Puja Chawla, SP Lochab, Nafa Singh (2011) Burstein Moss effect in nanocrystalline CaS: Ce Bull. Mater. Sci. 34(4), 673-676
16. Kim DT, Yu KS, Kim WT, Kim CD and Park HL (1992) Observation of Burstein-Moss shift in heavily copper-doped CaS:Cu phosphor. J. Mater. Sci. Lett. 11,886-887
17. Khalid M, Ziese M, Setzer A and Esquinazi P et al. (2009) Defect-induced magnetic order in pure ZnO films. Phys. Rev. B 80, 035331-035335.
18. Dole BN, Mote VD, Huse VR, Purushotham Y, Lande MK, Jadhav KM and Shah SS (2011) Structural studies of Mn doped ZnO nanoparticles. Curr. Appl. Phys.11, 762-e766
19. Bhatti KP, Chaudhary S, Pandya DK, and Kashyap SC (2005) Solid state commun. 136, 384-388.
20. Sharma VK, Xalxo R and Varma GD (2007) Structural and magnetic studies of Mn-doped ZnO. Cryst. Res. Tech. 42, 34–38.
21. Kajbafvala A, Shayegh MR, Mazloumi M, Zanganeh S, AidinLak SK, Sadrnezhaad J (2009) Alloys Compd. 469, 293-297.
22. Stroyuk AL, Kryukov AI, Kuchmiy S Ya, Pokhodenko VD (2005) Quantum size effects in semiconductor photo catalysis. Theor. Exp. Chem. 41(4), 207-228.
23. Viswanatha R, Sapra S, Gupta SS, Satpati B, Satyam PV, Dev BN, Sarma DD (2004) Synthesis and characterization of Mn-doped ZnOnanocrystals. J. Phys. Chem. B .108, 6303–6310
24. Reynolds DC, Look DC, Jogai B and Mokoc H (1997) Similarities in the bandedge and deep-centre photoluminescence mechanisms of ZnO and GaN. Solid State Commun.101, 643-646
25. Vimalkumara TV, Poornimaa N, Jineshb KB, SudhaKarthaa C and Vijayakumara KP (2011) On single doping and co-doping of spray pyrolysedZnO films: Structural, electrical and optical characterization Applied Surface Science 257, 8334-8340